Sensitivity and Noise Analysis of Resonant All-Fiber Optic Current Transformers

Zhiguo Jiang, Lixi Zhang, Guozhong Wang, and Lijun Jin

***Abstract*—The sensitivity and noise of an all-fiber optic current transformer (AFOCT) scheme named resonant AFOCT are analyzed, which senses the current information by measuring the frequency difference between clockwise and counterclockwise resonances inside a fiber ring resonator (FRR). Compared with polarization-type and interference-type AFOCT, the sensitivity of the resonant AFOCT can be improved by increasing the finesse of the FRR. The mathematical model of the resonant AFOCT is established, and the sensitivity expression of the resonant AFOCT limited by the sensitivity of the photodetector is derived. For the small current measurement of 1 mA level, the carrier suppression level of phase modulation is required to be better than $\rho_{ccw}\rho_{cw} = -110$ dB, and the intensity of unwanted polarization eigenstate of the FRR should be suppressed to less than −68 dBm. The non-ideal characteristics of fiber quarter-waveplate and the residual linear birefringence of spun fiber mainly affect the scale factor of the resonant AFOCT. The resonant AFOCT will be an important way to achieve high-precision of the current transformer.**

***Index Terms*—Optical fiber sensing, all-fiber optic current transformer, fiber ring resonator, sensitivity.**

I. Introduction

THE all-fiber optic current transformer (AFOCT) uses optical fiber as the sensing medium to measure the current based on the Faraday effect and Ampere's circuital law [1], [2]. Compared with traditional electromagnetic current transformers, the AFOCT has obvious advantages in miniaturization, safety, anti-electromagnetic interference, and transient performance [3], [4], [5], which is the key technology of ultra-high voltage power grid and smart grid.

According to the signal detection method, the existing AFOCT can be divided into polarization-type and interference-type. The polarization-type obtains the current information by directly detecting the rotation angle of the polarization plane of the linearly polarized light [1]. The interference-type obtains the current information by detecting the phase difference converted from the rotation angle of the polarization plane [2], [5], which can be subdivided into: Sagnac-gyro-type [2] and reflection-type [5].

The sensitivity is one of the important parameters of the AFOCT, and many studies have been done to improve the sensitivity of the AFOCT [6], [7], [8], [9]. Huang et al. presented a highly sensitive AFOCT using terbium doped fiber [6], and the Verdet constant of the terbium doped fiber at 1300 nm is found to be 19.5 μrad/A. However, the propagation loss of terbium doped fiber is high, which is estimated to be 0.08 dB/cm at 1300 nm, and the optimal length of terbium doped fiber in literature [6] is 0.5 meters. For even longer fibers, the exponential decrease of received optical power dominates over the linear increase in sensitivity [6]. Du et al. proposed an AFOCT based on recirculating fiber loop architecture for significantly enhancing the current sensitivity [7], and the recirculating loop is constructed by a 2 × 2 optical switch and the standard single mode fiber. Zhang et al. improved the sensitivity of the polarization-type AFOCT by allowing optical signals to traverse the sensor head repeatedly [8]. Since these methods using reentrant optical structures do not adopt reciprocal optical path design, it is difficult for the AFOCT to suppress the error caused by external environment. Maystre et al proposed a current transformer composed of discrete components [9], which employs a fiber-optic Fabry-Perot resonator. Wang et al proposed a resonant fiber optic gyroscope (RFOG) with counter-propagating circular polarization states [10], [11], which employs a fiber ring resonator (FRR) and has experimentally demonstrated that the device can also be operated as a current sensor, referred to as resonant AFOCT. The resonant AFOCT is based on multi beam interference effect, which senses the current information by measuring the frequency difference between clockwise (CW) and counterclockwise (CCW) resonances inside the FRR. Nevertheless, the noise and sensitivity models specific to the resonant AFOCT have not been fully established and analyzed in the existing work.

In this paper, we analyzed the sensitivity and noise of an resonant AFOCT. We established a mathematical model for resonant AFOCT and provided a detailed examination of its sensitivity, as well as the errors and noises caused by the non-ideal characteristics of fiber optic devices. Compared with the existing polarization-type and interferometric-type AFOCT, the sensitivity of the resonant AFOCT can be enhanced by increasing the finesse of the FRR. In theory, this approach facilitates the achievement of high-precision measurements.

Manuscript received 9 April 2024; accepted 3 June 2024. Date of publication 11 June 2024; date of current version 10 July 2024. This work was supported in part by the National Natural Science Foundation of China under Grant 52277157 and Grant U1966210 and in part by the Jiaxing Public Welfare Research Program Project under Grant 2022AY30021. *(Corresponding author: Lijun Jin.)*

Zhiguo Jiang is with the College of Electronic and Information Engineering, Tongji University, Shanghai 201806, China, and also with the Provincial Key Laboratory of Multimodal Perceiving and Intelligent Systems, Jiaxing University, Jiaxing 314001, China (e-mail: xidianzhiguo@163.com).

Lixi Zhang and Guozhong Wang are with the Zhejiang Fangyuan Electrical Equipment Testing Company, Ltd., Jiaxing 314001, China (e-mail: 387946976@qq.com; wgz667118@126.com).

Lijun Jin is with the College of Electronic and Information Engineering, Tongji University, Shanghai 201806, China (e-mail: jinlj@tongji.edu.cn).

Digital Object Identifier 10.1109/JPHOT.2024.3412237

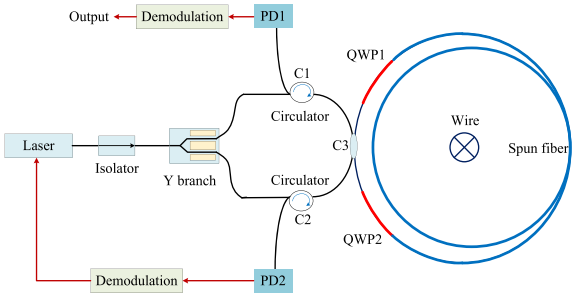

Fig. 1. Structure diagram of the resonant AFOCT.

II. Principles

A. Structure of Resonant AFOCT

The resonant AFOCT scheme is shown in Fig. 1, where all the fibers and couplers are polarization maintaining operation. It is worth noting that the structure of Sagnac-gyro-type AFOCT is similar to that of the interferometric fiber optic gyroscopes (IFOG), and the structure of the resonant AFOCT is similar to that of the RFOG. The difference is that the gyroscopes suppress various noises when measuring angular velocity, while the current transformers suppress various noises when measuring current.

In Fig. 1, the narrowband laser is divided into two waves after passing through the Y-waveguide. The two waves are phase modulated by the upper and lower arms of the Y-waveguide respectively, and then are launched into the FRR through the coupler C3 (single-axis operation) to form the CW and CCW waves. After the CW wave and CCW wave leave the FRR, they are coupled to photodetectors PD1 and PD2 by optical fiber circulators C1 and C2, respectively. The structure of the FRR in Fig. 1 is completely symmetrical, which can be called a circularly polarized FRR. Taking the CW direction as an example, the CW light wave passes through the quarter wave plate (QWP1), the spun fiber and the QWP2 successively in the FRR, and then enters the next circle after passing through the C3. One QWP is used to convert linearly polarized light to circularly polarized light, and the other QWP is used to restore circularly polarized light to linearly polarized light.

In Fig. 1, the upper and lower arms of the Y waveguide are loaded with triangular wave signals of different frequencies. The CCW path is the reference path, and the frequency of the laser source always tracks and locks the CCW resonant frequency of the FRR based on the triangular phase modulation and demodulation method [12], and the demodulation output signal at the PD2 is used to adjust the laser source frequency in real time. The CW path is the signal path, and the demodulation output signal at the PD1 is used to measure the difference between the CW resonant frequency and the laser source frequency, so as to obtain the frequency difference between the CW and CCW resonances, and then to obtain the current information.

B. Mathematical Model of Resonant AFOCT

To evaluate the performance of the resonant AFOCT, the model of the resonant AFOCT is derived. The input electric field $E(t)$ with finite temporal coherence can be denoted as

$$E(t) = E_0 \exp\left(-\mathrm{i}2\pi f_0 t - \mathrm{i}\phi\left(\mathrm{t}\right)\right) \tag{1}$$

where E_0 is the amplitude, f_0 is the center frequency of the laser, and $\phi(t)$ is a random initial phase. When the spectral distribution of the laser source follows Lorentz spectral line, there is a relationship $\left\langle \mathrm{e}^{-i\phi(t)} \cdot \mathrm{e}^{i\phi(t+\tau)} \right\rangle = \mathrm{e}^{-\pi\Delta\upsilon_L \cdot \tau}$, where $\Delta\upsilon_L$ is the laser linewidth, $\tau = n_e L/c$ is the time required for light to travel one cycle around the FRR, L is the cavity length of the FRR, n_e is the refractive index of the fiber, c is the speed of light.

The FRR is the sensing element of the resonant AFOCT, and its output electric field can be written as

$$\begin{bmatrix} E_{//0} \\ E_{\perp 0} \end{bmatrix} = \sqrt{1-K}\sqrt{1-\gamma}\left(1 - \frac{K}{1-K}\sum_{n=1}^{\infty}\left(S_N\right)^n\right) \times \begin{bmatrix} \cos\theta & -\sin\theta \\ \sqrt{\varepsilon}\sin\theta & \sqrt{\varepsilon}\cos\theta \end{bmatrix} \begin{bmatrix} E\left(t\right) \\ 0 \end{bmatrix} \tag{2}$$

where K is the coupling coefficient of the C3, γ is the insertion loss of the C3, ε is the extinction ratio of the C3, θ is the polarization crosstalk angle of the C3, $\begin{bmatrix} E_0 & 0 \end{bmatrix}^T$ is the input electric field of the FRR, and the transfer function S_N of the light propagating one circle along the FRR can be written as

$$S_N = R \cdot \mathrm{e}^{-\mathrm{i}2\pi f_0 \tau} \cdot \begin{bmatrix} \cos\theta & -\sin\theta \\ \sqrt{\varepsilon}\sin\theta & \sqrt{\varepsilon}\cos\theta \end{bmatrix} \cdot L_{Q2} \cdot L_F \cdot L_{Q1} \tag{3}$$

where $R = \sqrt{1-K}\sqrt{1-\gamma}\sqrt{1-\rho}$, ρ is the total insertion loss of the QWP1 and QWP2, L_{Q1}, L_{Q2} and L_F are the transfer function of the QWP1, the QWP2 and the spun fiber respectively.

In the FRR, due to the magnetic field generated by the measured current, the CW and CCW circularly polarized light will produce a phase difference φ when passing through the spun fiber. Referring to the principle of the interference-type AFOCT, the phase difference φ is equal to the polarization rotation $2F$ due to the Faraday effect. F can be written as

$$F = \frac{\varphi}{2} = NVI \tag{4}$$

where N is the number of turns of the sensing fiber, V is the Verdet constant, and I is the measured current. According to the properties of the FRR [13], [14], [15], (4) can be rewritten as

$$I = \frac{\varphi}{2 \cdot N \cdot V} = \frac{2\pi}{2 \cdot N \cdot V}\frac{\Delta f}{FSR} = \frac{\pi \cdot n_e \cdot L}{N \cdot V \cdot c}\Delta f \tag{5}$$

where $FSR = c/n_e L$ is the free spectral range of the FRR, and Δf is the frequency difference between the CW and CCW resonances. According to (5), the current I can be obtained by detecting the Δf.

Assuming that the C3, the QWP1, the QWP2 and the spun fiber are ideal, the output electric field E_{cw} in the clockwise direction of the FRR can be written as

$$E_{\mathrm{cw}} = E_0 \mathrm{e}^{-i2\pi f_0 t}\sqrt{1-\gamma} \times \left(\mathrm{e}^{-i\phi(\mathrm{t})}\sqrt{1-K} - \frac{K}{\sqrt{1-K}}\sum_{n=1}^{\infty}\mathrm{e}^{-i2\pi f_0 \tau n}\mathrm{e}^{-i\phi(t-n\tau)}R^n\right) \tag{6}$$

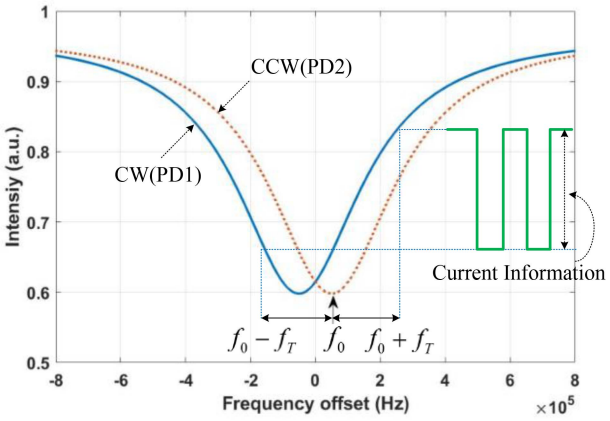

Fig. 2. CW and CCW resonance curves.

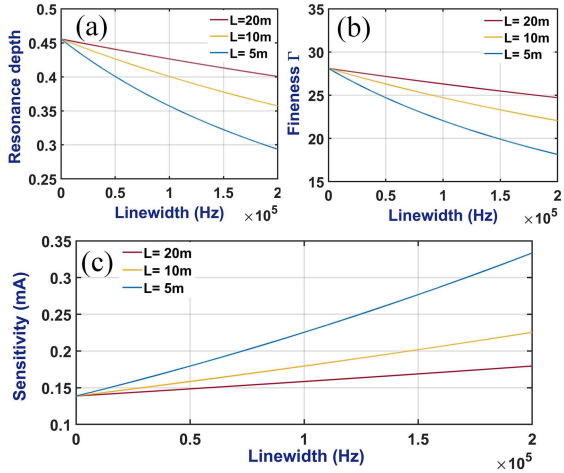

Fig. 3. Influence of linewidth on sensitivity.

The output intensity of the FRR with different laser source frequency can be derived as (7) and (8) shown at the bottom of this page, where T is the phase shift produced by circular birefringence of the spun fiber.

Fig. 2 shows the CW and CCW resonance curves of the FRR, where $f_0 + f_T$ and $f_0 - f_T$ are the frequencies corresponding to the first half cycle and the second half cycle of triangular phase modulation respectively. It can be shown that the existence of the polarization rotation F will separate the CW and CCW resonance curves, and the amplitude of the square wave output by the PD1 can be used to obtain the Δf information, and then to obtain the current I.

III. Sensitivity

The sensitivity expression of the resonant AFOCT is derived. Assuming that the working point frequency of the resonant AFOCT is near the maximum slope point of the resonant curve, according to the properties of the FRR [15], the change of its output optical intensity with the frequency f_0 can be approximately as $(P_{\max} - P_{\min})/\Delta f_{FWHM}$, where Δf_{FWHM} is the full width at half maximum of the resonance curve, and $P_{\max}$ and $P_{\min}$ are the maximum and minimum output optical intensity of the FRR respectively. Therefore, the minimum detectable current of the resonant AFOCT limited by the sensitivity of the photodetector can be derived as

$$I_S \approx \frac{\pi \cdot n_e \cdot L}{N \cdot V \cdot c} \frac{\Delta f_{\text{FWHM}}}{P_{\max} - P_{\min}} \sqrt{2} P_s$$

$$= \frac{\sqrt{2}\pi}{N \cdot V \cdot \Gamma} \frac{P_s}{P_{\max} - P_{\min}} \tag{9}$$

where $\sqrt{2}P_s$ is the noise equivalent power corresponding to two photodetectors, and $\Gamma = FSR/\Delta f_{FWHM}$ is the finesse of the FRR [14].

To achieve high finesse Γ, the FRR needs to satisfy an external condition that the coherence length of the laser source must be much greater than the cavity length of the FRR. The finesse $\Gamma$of the FRR can be derived as

$$\Gamma = \frac{\pi \sqrt{\sqrt{1-K}\sqrt{1-\gamma}\sqrt{1-\rho} \cdot \mathrm{e}^{-\pi \Delta \upsilon_L \cdot \frac{n_e L}{c}}}}{1 - \sqrt{1-K}\sqrt{1-\gamma}\sqrt{1-\rho} \cdot \mathrm{e}^{-\pi \Delta \upsilon_L \cdot \frac{n_e L}{c}}} \tag{10}$$

Obviously, when $\lim_{\Delta \upsilon_L \to 0} e^{-\pi \Delta \upsilon_L \cdot \tau} = 1, \Gamma = \pi\sqrt{R}/(1-R)$is obtained. It can be seen from (10) that the finesse Γ is mainly affected by the coupling coefficient K of the C3, the insertion loss γ and ρ, and the laser linewidth $\Delta \upsilon_L$.

Fig. 3 illustrates the influence of the linewidth on the finesseΓ, the resonance depth $(P_{\max} - P_{\min})$, and the sensitivity I_S, where $K = 0.03$, $\gamma = 0.03$, $\rho = 0.15$ [16], [17]. As the cavity length L increases and the linewidth $\Delta \upsilon_L$ decreases, there is a noticeable increase in the resonance depth, the finesse, and the sensitivity.

Fig. 4 illustrates the influence of the insertion loss on the finesseΓ, the resonance depth $(P_{\max} - P_{\min})$, and the sensitivity I_S, where $K = 0.03$, $\gamma = 0.03$, $\Delta \upsilon_L = 4\,\text{kHz}$, $L = 10\,\text{m}$. As the insertion loss ρ decreases, there is a noticeable increase in resonance depth, the finesse, and the sensitivity.

$$P_{\text{cw}} = E_0^2 (1-\gamma) \left\{ 1 - \frac{K}{1-R^2} \frac{(\gamma + \rho - \rho\gamma)\left(1 - \left(R\mathrm{e}^{-\pi \Delta \upsilon_L \tau}\right)^2\right)}{(1 - R\mathrm{e}^{-\pi \Delta \upsilon_L \tau})^2 + 4R\mathrm{e}^{-\pi \Delta \upsilon_L \tau} \sin^2\left(\frac{2\pi f_0 \tau + F + T}{2}\right)} \right\} \tag{7}$$

$$P_{\text{ccw}} = E_0^2 (1-\gamma) \left\{ 1 - \frac{K}{1-R^2} \frac{(\gamma + \rho - \rho\gamma)\left(1 - \left(R\mathrm{e}^{-\pi \Delta \upsilon_L \tau}\right)^2\right)}{(1 - R\mathrm{e}^{-\pi \Delta \upsilon_L \tau})^2 + 4R\mathrm{e}^{-\pi \Delta \upsilon_L \tau} \sin^2\left(\frac{2\pi f_0 \tau - F + T}{2}\right)} \right\} \tag{8}$$

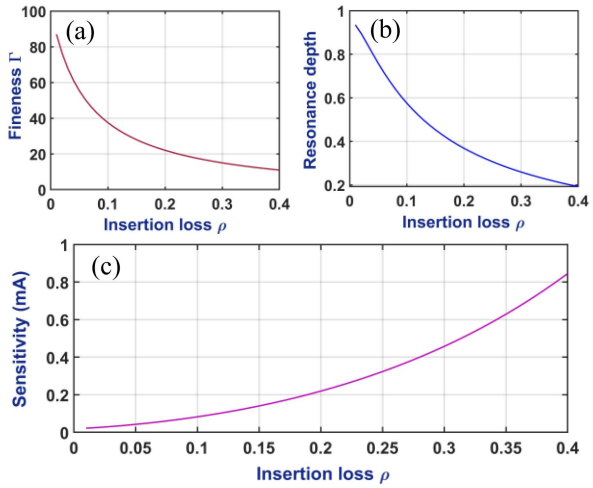

Fig. 4. Influence of insertion loss on sensitivity.

When $E_0^2 = 1\,\text{mW}$,$V = 10^{-6}\mu\text{rad/A}$, $\Gamma = 28$, $N = 25$, $P_s = 10\text{pW}$, the minimum detectable current of the AFOCT is about $I_S = 0.06\,\text{mA}$.

The minimum detectable current of the Sagnac-gyro-type AFOCT limited by the sensitivity of the photodetector can be derived as

$$I'_S = \frac{\pi}{2 \cdot V \cdot N} \cdot \frac{P_s}{P_{\max} - P_{\min}} \tag{11}$$

The sensitivity comparison between resonant AFOCT and Sagnac-gyro-type AFOCT is analogous to the sensitivity comparison between RFOG and IFOG [18]. The sensitivity of resonant AFOCT can be improved by winding more turns of fiber optic coils like a Sagnac-gyro-type AFOCT, and by circulating light multiple times within the FRR. By comparing (10) and (11), it can be seen that under the same number of sensing turns, the sensitivity of resonant AFOCT is $\Gamma/2\sqrt{2}$ times that of Sagnac gyro-type AFOCT. Currently, the finesse Γ generally ranges from 5 to 100. As a result, compared to Sagnac-gyro-type AFOCT, the sensitivity of the resonant AFOCT can be significantly enhanced.

According to (5), for a resonant AFOCT with a current sensitivity of 0.06mA, it is necessary to detect a frequency difference of 0.01Hz between the CW and CCW resonances of the FRR. Obviously, this frequency difference is extremely small. However, such a minute frequency difference is detectable. As per literature [19], the measurement accuracy of the RFOG has reached 0.02°/h, which corresponds to a frequency difference of 0.002 Hz between the CW and CCW resonances of the FRR. Its sensitivity is evidently less than 0.02°/h, indicating that 0.01Hz is indeed detectable.

IV. Error and Noise

The structure of the resonant AFOCT very similar to that of the RFOG. The noise and error sources of the resonant AFOCT include backscattering, polarization crosstalk of the coupler used to build the FRR, non-ideal characteristics of QWP, residual linear birefringence of spun fiber, the Kerr effect [20], [21], residual intensity modulation of the electro-optic phase modulator [22], and laser frequency noise [23]. Compared to the Kerr effect, the residual intensity modulation, and laser frequency noise, the backscattering and polarization crosstalk of the coupler have a more serious impact on the performance of the resonant AFOCT. Additionally, the non-ideal characteristics of QWP and residual linear birefringence of spun fiber are present in the resonant AFOCT and not present in the RFOG. Therefore, we analyzed the following noise and error sources in the paper, including the backscattering, polarization crosstalk of the coupler, non-ideal characteristics of QWP, and residual linear birefringence of spun fiber.

A. Backscattering

In the resonant AFOCT, a narrowband laser source is necessary to achieve high sensitivity, but it also introduces Rayleigh backscattering induced noise [24], [25]. Rayleigh backscattering is caused by the inhomogeneity of the optical fiber medium. As an estimate, the ensemble average intensity of the Rayleigh backscattering can be given by $I_r/I_0 \approx \alpha_R SL$, where α_R is fiber transmission loss, S is the recapture factor [26], [27]. In Fig. 1, the electric field of backscattering on the detector can be derived as [25]

$$E_r = E_0\sqrt{\alpha_R SL} \times K \sum_{m=0}^{\infty} R^m \mathrm{e}^{-\mathrm{i}m(2\pi f_0 \tau - F)} \times \sum_{n=0}^{\infty} R^n \mathrm{e}^{-\mathrm{i}n(2\pi f_0 \tau + F)} \tag{12}$$

The total intensity on the detector can be derived as

$$I_{r-s} = E_0^2 + 2E_r E_0 \cos(\Delta\xi) + E_r^2 \tag{13}$$

where $\Delta\xi$ is the phase difference between the backscattered light and signal light. It can be seen that the backscattering induced noise includes the backscattering intensity itself and the interference term, and the interference term noise is relatively heavier.

Referring to the RFOG, the intensity-term noise can be suppressed by phase modulation and demodulation with different frequencies in the CW and CCW directions [12]. The interference-term noise can be reduced by the carrier-suppressed phase modulation technique [12], and the effectiveness of the technique is determined by the carrier suppression level. With the carrier-suppressed phase modulation, the maximum amplitude of interference-term noise can be derived as

$$I_{i-\max} = (2E_r E_0 \cos(\Delta\xi))_{\max} = \frac{2E_0^2\sqrt{\alpha_R SL} \cdot K}{(1-R)^2}\sqrt{\rho_{\text{ccw}}\rho_{\text{cw}}} \tag{14}$$

where ρ_{cw} and ρ_{ccw} are the carrier suppression levels of the phase modulation in the CW and CCW direction respectively. When$E_0^2 = 1\,\text{mW}$, $\alpha_R = 0.2\,\text{dB/km}$, $S = 10^{-3}$ [26],

[27], L= 10 m, $\gamma = 0.03$ and$K = 0.03$, the maximum amplitude of the interference-term noise is $0.056\sqrt{\rho_{\mathrm{ccw}}\rho_{\mathrm{cw}}}$ mW. According to (9), when the measured current is 1mA, the amplitude of the signal on the detector is 160 pW (−68 dBm). Therefore, in order to measure small current of 1mA level, the requirement of the carrier suppression level of the phase modulation should be better than $\rho_{\mathrm{ccw}}\rho_{\mathrm{cw}}$= − 110 dB.

B. Polarization Crosstalk of Coupler

In the resonant AFOCT, the polarization fluctuation induced error is caused by the non-ideal characteristics of optical fiber devices. There are two eigenstates of polarization in the FRR [28], corresponding to two resonance peaks. The temperature change will make the two resonance peaks overlap, resulting in the instability of the symmetry of the primary resonance peak, which introduce an error in the detection of the center frequency of the primary resonance, thus affecting the bias drift of the resonant AFOCT.

The polarization fluctuation induced error can be suppressed by attenuating the intensity of unwanted polarization eigenstate [28], [29]. However, the polarization crosstalk of the coupler C3 reduce the effectiveness of this suppression method. In Fig. 1, the transfer Jones matrix of the light propagating one circle along the CW direction of the FRR can be written as

$$S_{N-\mathrm{cw}} = R\cdot \mathrm{e}^{-\mathrm{i}2\pi f_0\tau}\cdot \mathrm{e}^{-\mathrm{i}(F+T)}\begin{bmatrix}\cos\theta & -\sin\theta\\ \sqrt{\varepsilon}\sin\theta & \sqrt{\varepsilon}\cos\theta\end{bmatrix} \tag{15}$$

where the QWP1, the QWP2 and the spun fiber are assumed to be ideal.

According to the properties of the matrix, the transfer matrix $S_{N-\mathrm{cw}}$ has two eigenvalues and two eigenvectors, which correspond to the two eigenstates of polarization in the FRR [28]. The eigenvalues and eigenvectors can be written as

$$R\cdot \mathrm{e}^{-\mathrm{i}2\pi f_0\tau}\mathrm{e}^{-\mathrm{i}(F+T)}\begin{bmatrix}\cos\theta & -\sin\theta\\ \sqrt{\varepsilon}\sin\theta & \sqrt{\varepsilon}\cos\theta\end{bmatrix}\cdot\begin{bmatrix}1\\ b_{1,2}\end{bmatrix} = \lambda_{1,2}\cdot\begin{bmatrix}1\\ b_{1,2}\end{bmatrix} \tag{16}$$

where λ_1 and λ_2 are two eigenvalues, $\begin{bmatrix}1 & b_1\end{bmatrix}^T$ and $\begin{bmatrix}1 & b_2\end{bmatrix}^T$ are two eigenvectors.

The energy of the input electric field of the FRR is assigned to two eigenvectors, and the input electric field can be rewritten as

$$\begin{bmatrix}\cos\theta & -\sin\theta\\ \sqrt{\varepsilon}\sin\theta & \sqrt{\varepsilon}\cos\theta\end{bmatrix}\cdot\begin{bmatrix}1\\ 0\end{bmatrix} = X_1\begin{bmatrix}1\\ b_1\end{bmatrix} + X_2\begin{bmatrix}1\\ b_2\end{bmatrix} \tag{17}$$

where X_1 and X_2 are the coefficients.

After derivation, λ_1, λ_2, b_1, b_2, X_1 and X_2 can be written as

$$\lambda_1 = R\cdot \mathrm{e}^{-\mathrm{i}2\pi f_0\tau}\mathrm{e}^{-\mathrm{i}(F+T)}\times\frac{(\sqrt{\varepsilon}+1)\cos\theta-\sqrt{(1-\sqrt{\varepsilon})^2\cos^2\theta-4\sqrt{\varepsilon}\sin^2\theta}}{2}$$

$$\lambda_2 = R\cdot \mathrm{e}^{-\mathrm{i}2\pi f_0\tau}\mathrm{e}^{-\mathrm{i}(F+T)}\times\frac{(\sqrt{\varepsilon}+1)\cos\theta+\sqrt{(1-\sqrt{\varepsilon})^2\cos^2\theta-4\sqrt{\varepsilon}\sin^2\theta}}{2}$$

$$b_1 = \frac{(1-\sqrt{\varepsilon})\cos\theta+\sqrt{(1-\sqrt{\varepsilon})^2\cos^2\theta-4\sqrt{\varepsilon}\sin^2\theta}}{2\sin\theta}$$

$$b_2 = \frac{(1-\sqrt{\varepsilon})\cos\theta-\sqrt{(1-\sqrt{\varepsilon})^2\cos^2\theta-4\sqrt{\varepsilon}\sin^2\theta}}{2\sin\theta}$$

$$X_1 = \frac{\sqrt{\varepsilon}\left(1+\sin^2\theta\right)-\cos^2\theta+\cos\theta\sqrt{(1-\sqrt{\varepsilon})^2\cos^2\theta-4\sqrt{\varepsilon}\sin^2\theta}}{2\sqrt{(1-\sqrt{\varepsilon})^2\cos^2\theta-4\sqrt{\varepsilon}\sin^2\theta}}$$

$$X_2 = \frac{-\sqrt{\varepsilon}\left(1+\sin^2\theta\right)+\cos^2\theta+\cos\theta\sqrt{(1-\sqrt{\varepsilon})^2\cos^2\theta-4\sqrt{\varepsilon}\sin^2\theta}}{2\sqrt{(1-\sqrt{\varepsilon})^2\cos^2\theta-4\sqrt{\varepsilon}\sin^2\theta}} \tag{18}$$

Therefore, the output intensity of the two polarization eigenstates of the FRR can be written as

$$\begin{aligned} I_{ESOP1} &= \left|R-\tfrac{K\sqrt{1-\gamma}}{\sqrt{1-K}}\tfrac{\lambda_1}{1-\lambda_1}\right|^2 X_1X_1^*\begin{bmatrix}1\\ b_1\end{bmatrix}^H\begin{bmatrix}1\\ b_1\end{bmatrix}\\ I_{ESOP2} &= \left|R-\tfrac{K\sqrt{1-\gamma}}{\sqrt{1-K}}\tfrac{\lambda_2}{1-\lambda_2}\right|^2 X_2X_2^*\begin{bmatrix}1\\ b_2\end{bmatrix}^H\begin{bmatrix}1\\ b_2\end{bmatrix}\end{aligned} \tag{19}$$

The ratio of the intensities of the two polarization eigenstates can be written as

$$\frac{I_{ESOP1}}{I_{ESOP2}} = \frac{|X_1|^2\left(1+|b_1|^2\right)}{|X_2|^2\left(1+|b_2|^2\right)} \tag{20}$$

In fact, most of the energy will be assigned to the primary polarization eigenstate, so $|X_2|^2(1+|b_2|^2)\approx 1$. Therefore, the output intensity of unwanted polarization eigenstate can be written as

$$I_{un}\approx\frac{E_0^2}{4}\left(\begin{array}{l}\left|\frac{\sqrt{\varepsilon}\left(1+\sin^2\theta\right)-\cos^2\theta}{\sqrt{(1-\sqrt{\varepsilon})^2\cos^2\theta-4\sqrt{\varepsilon}\sin^2\theta}}+\cos\theta\right|^2+\\ \varepsilon\left|\frac{-(1+\sqrt{\varepsilon})\sin\theta\cos\theta}{\sqrt{(1-\sqrt{\varepsilon})^2\cos^2\theta-4\sqrt{\varepsilon}\sin^2\theta}}+\sin\theta\right|^2\end{array}\right) \tag{21}$$

Fig. 5 shows the intensity of unwanted polarization eigenstate, where $E_0^2 = 1$ mW. According to (9), when the measured current is 1mA, the amplitude of the signal on the detector is 160 pW (−68 dBm). The extinction ratio ε and polarization crosstalk angle θ of commercially available couplers are approximately −25 dB and 6 degrees [16], [17], respectively. Referring to Fig. 5, the corresponding intensity of unwanted polarization eigenstate is less than −68 dBm, thus meeting the measurement requirement of 1mA current.

C. Non-Ideal Characteristics of QWP

In the resonant AFOCT, the nonreciprocal phase shift is accumulated by circularly polarized light waves, and it is necessary to produce high-quality states of circular polarization. However, it should be noted that it is very difficult to design a QWP that maintains a high quality over a large temperature range [30]. The non-ideal characteristics of the QWP refer to the deviation of the principal axis angle δ and phase retardation ϕ by 45° and 90° respectively. The transfer Jones matrix of the light propagating one circle along the CW direction of the FRR can be written as

$$\begin{aligned} S_{N-\mathrm{cw}} = R \cdot \mathrm{e}^{-\mathrm{i}2\pi f_0 \tau} & \begin{bmatrix} \cos\theta_2 & -\sin\theta_2 e^{i\phi_2} \\ 0 & 0 \end{bmatrix} \\ & \times \begin{bmatrix} \cos(T+F) & -\sin(T+F) \\ \sin(T+F) & \cos(T+F) \end{bmatrix} \\ & \times \begin{bmatrix} \cos\theta_1 & -\sin\theta_1 \\ \sin\theta_1 e^{i\phi_1} & \cos\theta_1 e^{i\phi_1} \end{bmatrix} \end{aligned} \tag{22}$$

where the coupler C3 and the spun fiber are assumed to be ideal, θ_1 and ϕ_1 are the principal axis angle and phase retardation of the QWP1 respectively, θ_2 and ϕ_2 are the principal axis angle and phase retardation of the QWP2 respectively.

According to the properties of the matrix, the eigenvalues of the transfer matrix $S_{N-\mathrm{cw}}$ can be written as

$$\begin{aligned} \lambda_{1\mathrm{cw}} &= \lambda_{2\mathrm{cw}} \\ &= R \cdot \mathrm{e}^{-\mathrm{i}2\pi f_0 \tau} \begin{pmatrix} \begin{pmatrix} \cos(T+F)\cos\theta_1\cos\theta_2 - \\ \sin(T+F)\sin\theta_1\cos\theta_2 e^{i\phi_1} \end{pmatrix} \\ \begin{pmatrix} -\sin(T+F)\cos\theta_1\sin\theta_2 e^{i\phi_2} - \\ \cos(T+F)\sin\theta_1\sin\theta_2 e^{i\phi_1} e^{i\phi_2} \end{pmatrix} \end{pmatrix} \end{aligned} \tag{23}$$

which indicates that only one eigenstate of polarization will be excited in the CW direction, and the phase angle of the eigenvalue can be written as (24) shown at the bottom of this page.

Similarly, the phase angle of the eigenvalue in the CCW direction can be written as (25) shown at the bottom of this page.

The frequency difference between the CW and CCW directions can be written as

$$\Delta f = \frac{c}{2n_e L\pi}\left(\vartheta_{\mathrm{cw}} - \vartheta_{\mathrm{ccw}}\right) \tag{26}$$

As can be seen, if $F = 0$, then $\Delta f = 0$. Therefore, the non-ideal characteristics of the QWP mainly affects the scale factor. For current measurements of 1mA and 1kA, when $\theta_1 - \theta_2 = 2^\circ$ and $\phi_2 - \phi_1 = 8^\circ$ [31], the scale factors for the measurements are 0.18% and 0.18%, respectively.

D. Residual Linear Birefringence of Spun Fiber

In the resonant AFOCT, the residual linear birefringence of the spun fiber also introduces polarization rotation, resulting in an error signal that cannot be distinguished from the Faraday rotation [32], [33], [34]. Considering the linear birefringence of the spun fiber, the transfer Jones matrix of the light propagating one circle along the CW direction of the FRR can be written as (27) shown at the top of the next page, where the coupler C3, the QWP1 and the QWP2 are assumed to be ideal, and $\alpha = 2\sqrt{(\nu/2)^2 + (T+F)^2}$, $\chi = \arctan(2(T+F)/\nu)$ [33], [34], ν is the phase shift produced by linear birefringence of the spun fiber.

According to the properties of the matrix, the eigenvalues of the transfer matrix $S_{N-\mathrm{cw}}$ can be written as

$$\lambda'_{1\mathrm{cw}} = \lambda'_{2\mathrm{cw}} = R \cdot \mathrm{e}^{-\mathrm{i}2\pi f_0 \tau}\left(\cos\frac{\alpha}{2} - i\sin\frac{\alpha}{2}\sin\chi\right) \tag{28}$$

which indicates that only one eigenstate of polarization will be excited in the CW direction, and the phase angle of the eigenvalue can be written as

$$\vartheta'_{\mathrm{cw}} = \arctan\left(-\tan\frac{\alpha}{2}\sin\chi\right) \tag{29}$$

Similarly, the phase angle of the eigenvalue in the CCW direction can be written as

$$\vartheta'_{\mathrm{ccw}} = \arctan\left(-\tan\frac{\beta}{2}\sin\xi\right) \tag{30}$$

where $\beta = 2\sqrt{(\nu/2)^2 + (T-F)^2}$, $\xi = arctan(2(T-F)/\nu)$ [33], [34].

Considering the residual linear birefringence of the spun fiber, the frequency difference between the CW and CCW directions can be written as

$$\begin{aligned} \Delta f = & \frac{c}{2n_e L\pi} \\ & \times \left(\arctan\left(-\tan\frac{\alpha}{2}\sin\chi\right) - \arctan\left(-\tan\frac{\beta}{2}\sin\xi\right)\right) \end{aligned} \tag{31}$$

As can be seen, if $F = 0$, then $\Delta f = 0$. Therefore, the residual linear birefringence of the spun fiber mainly affects the scale factor. [35], [36] indicate that the circular and linear birefringence

$$\vartheta_{\mathrm{cw}} = \arctan\frac{\sin(\theta_1-\theta_2)\sin\left(\frac{\phi_1-\phi_2}{2}\right)\tan(T+F) + \cos(\theta_1-\theta_2)\sin\left(\frac{\phi_1+\phi_2}{2}\right)}{\sin(\theta_1+\theta_2)\cos\left(\frac{\phi_1-\phi_2}{2}\right)\tan(T+F) - \cos(\theta_1+\theta_2)\cos\left(\frac{\phi_1+\phi_2}{2}\right)} \tag{24}$$

$$\vartheta_{\mathrm{ccw}} = \arctan\frac{\sin(\theta_1-\theta_2)\sin\left(\frac{\phi_1-\phi_2}{2}\right)\tan(T-F) + \cos(\theta_1-\theta_2)\sin\left(\frac{\phi_1+\phi_2}{2}\right)}{\sin(\theta_1+\theta_2)\cos\left(\frac{\phi_1-\phi_2}{2}\right)\tan(T-F) - \cos(\theta_1+\theta_2)\cos\left(\frac{\phi_1+\phi_2}{2}\right)} \tag{25}$$

$$S_{N-\mathrm{cw}} = R \cdot \mathrm{e}^{-\mathrm{i}2\pi f_0 \tau} \frac{1}{2} \times \begin{bmatrix} \cos\frac{\alpha}{2} + i\sin\frac{\alpha}{2}\cos\chi - i\sin\frac{\alpha}{2}\sin\chi & -\sin\frac{\alpha}{2}\sin\chi - i\cos\frac{\alpha}{2} - \sin\frac{\alpha}{2}\cos\chi \\ 0 & 0 \end{bmatrix} \begin{bmatrix} 1 & -1 \\ \mathrm{i} & \mathrm{i} \end{bmatrix} \tag{27}$$

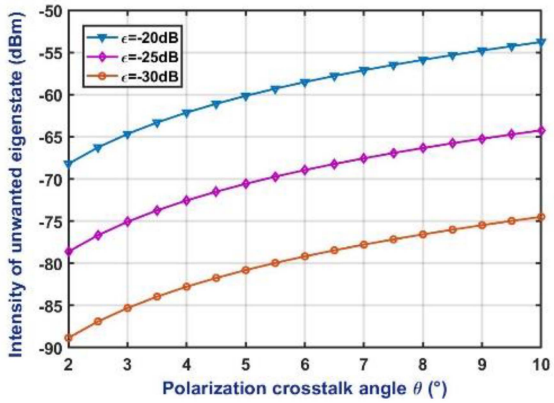

Fig. 5. Intensity of the unwanted polarization eigenstate.

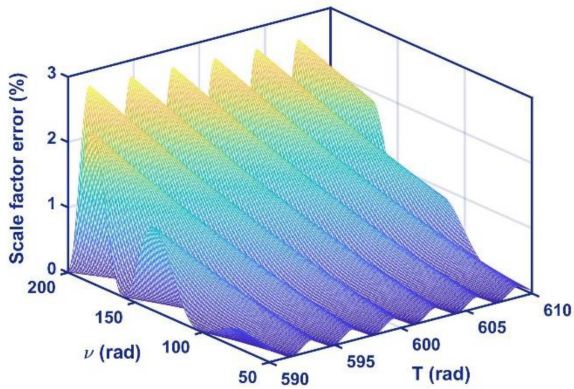

Fig. 6. Influence of the residual linear birefringence on scale factor error.

of a 10-meter commercial spun fiber are approximately 600 and 150, respectively. Fig. 6 illustrates the scale factor error as a function of the linear birefringence and circular birefringence when the measured current is 1mA. As can be seen from Fig. 6, the introduction of a large number of circular birefringence can suppress the scale factor error caused by residual linear birefringence.

V. Conclusion

In conclusion, an AFOCT scheme employing a FRR is analyzed, and the influences of non-ideal characteristics of optical devices on the performance of the resonant AFOCT are present. Compared with Sagnac-gyro-type AFOCT, the number of turns of the sensing fiber wound on the wire in the resonant AFOCT can be reduced by $\Gamma/2\sqrt{2}$ times under the same sensitivity. For the small current measurement of 1mA level, the carrier suppression level of phase modulation is required to be better than $\rho_{\mathrm{ccw}}\rho_{\mathrm{cw}} = -110\,\mathrm{dB}$, and the intensity of unwanted polarization eigenstate of the FRR should be suppressed to less than -68 dBm. The non-ideal characteristics of QWP and the residual linear birefringence of spun fiber mainly affect the scale factor of the resonant AFOCT. The resonant AFOCT will be an important way to achieve high-precision of the current transformer.

References

[1] A. Madaschi, M. Brunero, M. Ferrario, P. Martelli, P. Boffi, and M. Martinelli, "Experimental evaluation of the birefringence effect on faraday-based Fiber-optic current sensors," *IEEE Sensors Lett.*, vol. 6, no. 6, Jun. 2022, Art. no. 5000404, doi: 10.1109/LSENS.2022.3174079.

[2] J. Wu and X. Zhang, "Recent progress of all fiber optic current transformers," in *Proc. IEEE 7th Int. Forum Elect. Eng. Automat.*, 2020, pp. 134–143.

[3] Y. Huang, L. Xia, F. Pang, Y. Yuan, and J. Ji, "Self-compensative fiber optic current sensor," *J. Lightw. Technol.*, vol. 39, no. 7, pp. 2187–2193, Apr. 2021, doi: 10.1109/JLT.2020.3044935.

[4] K. Bohnert, A. Frank, L. Yang, X. Gu, and G. M. Müller, "Polarimetric fiber-optic current sensor with integrated-optic polarization splitter," *J. Lightw. Technol.*, vol. 37, no. 14, pp. 3672–3678, Jul. 2019, doi: 10.1109/JLT.2019.2919387.

[5] B. Liu et al., "Research on step response characteristics of flexible DC fiber-optic current transformer," in *Proc. IEEE Int. Conf. Signal, Inf. Data Process.*, 2019, pp. 1–5.

[6] D. Huang, S. Srinivasan, and J. E. Bowers, "Compact Tb doped fiber optic current sensor with high sensitivity," *Opt. Exp.*, vol. 23, no. 23, pp. 29993–29999, 2015, doi: 10.1364/OE.23.029993.

[7] J. Du, Y. Tao, Y. Liu, L. Ma, W. Zhang, and Z. He, "Highly sensitive and reconfigurable fiber optic current sensor by optical recirculating in a fiber loop," *Opt. Exp.*, vol. 24, no. 16, pp. 17980–17988, 2016, doi: 10.1364/OE.24.017980.

[8] H. Zhang, Y. Qiu, H. Li, A. Huang, H. Chen, and G. Li, "High-current-sensitivity all-fiber current sensor based on fiber loop architecture," *Opt. Exp.*, vol. 20, no. 17, pp. 18591–18599, 2012, doi: 10.1364/OE.20.018591.

[9] F. Maystre and A. Bertholds, "Magneto-optic current sensor using a helical-fiber Fabry–Perot resonator," *Opt. Lett.*, 1989, vol. 14, no. 11, pp. 587–589, doi: 10.1364/OL.14.000587.

[10] Z. Wang, G. Wang, W. Miao, W. Gao, and Y. Cheng, "Closed-loop method based on Faraday effect in resonant fiber optic gyro employing a low coherence-noise resonator," *J. Lightw. Technol.*, vol. 39, no. 21, pp. 6994–7000, Nov. 2021, doi: 10.1109/JLT.2021.3108005.

[11] Z. Wang, G. Wang, Z. Wang, W. Gao, and Y. Cheng, "Incoherence suppression method of optical noises in a resonant fiber optic gyro based on the circularly polarized light propagation mechanism in a resonator," *Opt. Lett.*, vol. 46, no. 13, pp. 3191–3194, 2021, doi: 10.1364/OL.431065.

[12] H. Ma, J. Zhang, L. Wang, and Z. Jin, "Development and evaluation of optical passive resonant gyroscopes," *J. Lightw. Technol.*, vol. 35, no. 16, pp. 3546–3554, Aug. 2017, doi: 10.1109/JLT.2016.2587667.

[13] D. M. Shupe, "Fiber resonator gyroscope: Sensitivity and thermal nonreciprocity," *Appl. Opt.*, vol. 20, no. 2, pp. 286–289, 1981, doi: 10.1364/AO.20.000286.

[14] L. F. Stokes, M. Chodorow, and H. J. Shaw, "All-single-mode fiber resonator," *Opt. Lett.*, vol. 7, no. 6, pp. 288–290, 1982, doi: 10.1364/OL.7.000288.

[15] Z. G. Jiang and Z. F. Hu, "Analysis on sensitivity of resonant fiber optic gyro," *Chin. J. Lasers*, vol. 44, no. 7, pp. 311–317, 2017, doi: 10.3788/CJL201744.0706001.

[16] H. Liu, W. Wang, J. Wang, L. Feng, and Y. Zhi, "In-line polarizer used in all-0°-splice resonator fiber-optic gyro," *Appl. Opt.*, vol. 52, no. 32, pp. 7821–7825, 2013, doi: 10.1364/AO.52.007821.

[17] H. Ma, X. Yu, and Z. Jin, "Reduction of polarization-fluctuation induced drift in resonator fiber optic gyro by a resonator integrating in-line polarizers," *Opt. Lett.*, vol. 37, no. 16, pp. 3342–3344, 2012, doi: 10.1364/OL.37.003342.

[18] R. Carroll et al., "The passive resonator fiber optic gyro and comparison to the interferometer fiber gyro," *Proc. SPIE*, vol. 719, pp. 169–177, 1987.

[19] G. A. Sanders, L. K. Strandjord, W. Williams, E. Benser, S. Ayotte, and F. Costin, "Improvements to signal processing and component miniaturization of compact resonator fiber optic gyroscopes," in *Proc. IEEE DGON Inertial Sensors Syst.*, 2018, pp. 1–22, doi: 10.1109/InertialSensors.2018.8577190.

[20] H. Ma et al., "Reduction of optical Kerr-effect induced error in a resonant micro-optic gyro by light-intensity feedback technique," *Appl. Opt.*, vol. 53, no. 16, pp. 3465–3472, 2014, doi: 10.1364/AO.53.003465.

[21] X. Li, J. Zhang, H. Ma, and Z. Jin, "Test and analysis of the optical Kerr-effect in resonant micro-optic gyros," *IEEE Photon. J.*, vol. 6, no. 5, Oct. 2014, Art. no. 6601007, doi: 10.1109/JPHOT.2014.2352635.

[22] C. Zhang et al., "Suppression of residual intensity modulation noise in resonator integrated optic gyro," *Opt. Commun.*, vol. 430, pp. 358–363, 2019, doi: 10.1016/j.optcom.2018.08.059.

[23] H. Ma et al., "Laser frequency noise induced error in resonant fiber optic gyro due to an intermodulation effect," *Opt. Exp.*, vol. 23, no. 20, pp. 25474–25486, 2015, doi: 10.1364/OE.23.025474.

[24] K. Iwatsuki, K. Hotate, and M. Higashiguchi, "Effect of Rayleigh backscattering in an optical passive ring-resonator gyro," *Appl. Opt.*, vol. 23, no. 21, pp. 3916–3924, 1984, doi: 10.1364/AO.23.003916.

[25] Z. G. Jiang, Z. F. Hu, and C. S. Fu, "Angular random walk limited by Rayleigh backscattering in resonator fiber optic gyros," *Appl. Opt.*, vol. 56, no. 34, pp. 9414–9422, 2017, doi: 10.1364/AO.56.009414.

[26] H. Ma et al., "Full investigation of the backscattering in resonator fiber optic gyro," *Opt. Commun.*, vol. 284, no. 19, pp. 4480–4484, 2011, doi: 10.1016/j.optcom.2011.06.018.

[27] M. Artiglia, M. A. Locaputo, and C. Ruocchio, "Backscattering recapture factor measurements using optical continuous wave reflectometry," in *Proc. IEEE 28TH Eur. Conf. Opt. Commun.*, 2002, pp. 1–2.

[28] K. Hotate and M. Higashiguchi, "Eigenstate of polarization in a fiber ring resonator and its effect in an optical passive ring-resonator gyro," *Appl. Opt.*, vol. 25, no. 15, pp. 2606–2612, 1986, doi: 10.1364/AO.25.002606.

[29] K. Takiguchi and K. Hotate, "Bias of an optical passive ring-resonator gyro caused by the misalignment of the polarization axis in the polarization-maintaining fiber resonator," *J. Lightw. Technol.*, vol. 10, no. 4, pp. 514–522, Apr. 1992, doi: 10.1109/50.134206.

[30] S. X. Short, A. A. Tselikov, J. U. de Arruda, and J. N. Blake, "Imperfect quarter-waveplate compensation in Sagnac interferometer-type current sensors," *J. Lightw. Technol.*, vol. 16, no. 7, pp. 1212–1219, Jul. 1998, doi: 10.1109/50.701399.

[31] R. Zhang et al., "Polarization-maintaining photonic crystal fiber based quarter waveplate for temperature stability improvement of fiber optic current sensor," *J. Modern Opt.*, vol. 60, no. 12, pp. 963–969, 2013, doi: 10.1080/09500340.2013.825335.

[32] H. Gao et al., "A chiral photonic crystal fiber sensing coil for decreasing the polarization error in a fiber optic current sensor," *Opt. Commun.*, vol. 469, 2020, Art. no. 125755, doi: 10.1016/j.optcom.2020.125755.

[33] S. X. Short, J. U. De Arruda, A. A. Tselikov, and J. N. Blake, "Elimination of birefringence induced scale factor errors in the in-line Sagnac interferometer current sensor," *J. Lightw. Technol.*, vol. 16, no. 10, pp. 1844–1850, Oct. 1998, doi: 10.1109/50.721071.

[34] P. R. Forman and F. C. Jahoda, "Linear birefringence effects on fiber-optic current sensors," *Appl. Opt.*, vol. 27, no. 15, pp. 3088–3096, 1998, doi: 10.1364/AO.27.003088.

[35] Z. Xu et al., "Accurate measurements of circular and residual linear birefringences of spun fibers using binary polarization rotators," *Opt. Exp.*, vol. 25, no. 24, pp. 30780–30792, 2017, doi: 10.1364/OE.25.030780.

[36] P. Yao et al., "Relative error's quadratic dependence on the electric current and the methods for its compensation in fiber optic current sensor systems," *Opt. Exp.*, vol. 30, no. 25, pp. 45471–45487, 2022, doi: 10.1364/OE.475731.